Project Report
LSP-377

Enabling Tech for Mid-IR Free-Space Optical Communications: FY23 Advanced Devices Line-Supported Program

K.J. Creedon
J.D. Moores
S. Ramakrishnan
T. Williams
B. Reynolds
W. Gerych
J.R. Norstrom
G.M. Smith
L.J. Missaggia
M.K. Connors
J.G. Cederberg
F.N. Jose
W. Shin
L. Ladas

28 February 2024

Lincoln Laboratory
MASSACHUSETTS INSTITUTE OF TECHNOLOGY
LEXINGTON, MASSACHUSETTS

This material is based upon work supported by the Under Secretary of Defense for Research and Engineering under Air Force Contract No. FA8702-15-D-0001.

This report is the result of studies performed at Lincoln Laboratory, a federally funded research and development center operated by Massachusetts Institute of Technology. This material is based upon work supported by the Under Secretary of Defense for Research and Engineering under Air Force Contract No. FA8702-15-D-0001. Any opinions, findings, conclusions or recommendations expressed in this material are those of the author(s) and do not necessarily reflect the views of the Under Secretary of Defense for Research and Engineering.

Massachusetts Institute of Technology
Lincoln Laboratory

Enabling Tech for Mid-IR Free-Space Optical Communications: FY23 Advanced Devices Line-Supported Program

K.J. Creedon
J.R. Norstrom
G.M. Smith
L.J. Missaggia
M.K. Connors
J.G. Cederberg
F.N. Jose
W. Shin
Group 82

J.D. Moores
S. Ramakrishnan
B. Reynolds
Group 66

T. Williams

W. Gerych
WPI

L. Ladas
University of Rochester

Project Report LSP-377

28 February 2024

This material is based upon work supported by the Under Secretary of Defense for Research and Engineering under Air Force Contract No. FA8702-15-D-0001.

Lexington Massachusetts

This page intentionally left blank.

TABLE OF CONTENTS

This page intentionally left blank.

LIST OF FIGURES

1. INTRODUCTION AND MOTIVATION

1.1 CONCEPT OVERVIEW

Free space optical communication (FSOC) systems have several inherent advantages over radio frequency (RF) in terms of achievable data rates, bandwidth utilization, and, particularly, for improved directionality, which reduces probability of detection, and of data interception. Historically, such systems have typically operated in the 1.0 and 1.55 μm near-infrared (NIR) and short-wave infrared (SWIR) wavelength bands, originally developed for compatibility with commercially available high-power optical amplifiers (rare-earth doped, solid state, or optical fiber), and availability of other components such as efficient modulators, detectors, and fiber optics. Though there have been suggestions that mid-wave infrared (MWIR) wavelength bands could offer reduced atmospheric impairments [1], relatively little development has occurred due to the lack of a commercially available component base compared to the NIR and SWIR. To address this gap, this project seeks to develop both an underlying laser transmitter technology and a practical understanding of the channel characteristics to lay out a path to a scalable, tactical communications system.

There exists a strong body of theoretical work in the literature that suggests a longer infrared wavelength reduces both the scintillation and scattering of an infrared beam propagating through a free-space atmospheric channel. Scintillation in this context describes the spatiotemporal irradiance fluctuations of a transmitted beam attributable to the random variations of the refractive index in air. Atmospheric attenuation is attributed to the scattering and absorption of light from molecular and aerosol sources. In addition, any optical beam propagated through a channel experiences an effective attenuation known as spreading loss when the receive aperture area is less than the area of the beam at the receive plane, which is typically the case for FSOC. A perceived downside of longer wavelengths is that the diffraction is stronger. However, 1.55 μm light has been used for Earth-geosynchronous lasercom (NASA's LCRD; 37 Mm) and even for Earth–Moon lasercom (NASA's LLCD; 400 Mm), here we are primarily targeting tactical applications with ranges of tens of km. Rather than being a detriment, broader, more highly diffracted beams can be expected to improve robustness of tactical links and facilitate link acquisition with maneuvering platforms. In tactical scenarios, diffractive losses are expected to be less important than sensitivity to weather conditions. One of the goals of this project is to quantify this difference with real, outdoor experimental data.

1.2 REPORT SUMMARY

Over a three-year development effort, we have demonstrated a novel laser architecture for high-speed amplitude modulation of quantum cascade laser (QCL) sources, building a master oscillator power amplifier (MOPA) testbed based on long-wave infrared (LWIR) devices near 9 μm that were grown, fabricated, coated, and packaged in house. Through systems studies and atmospheric measurements, we concluded that there were significant advantages to operating at slightly shorter wavelengths, and developed

the basic components needed to apply this architecture in the MWIR. This development included growing and fabricating laser epitaxy emitting between 4.0 and 5.0 μm, and developing facet coating recipes to enable device operation as either laser oscillators or amplifiers. In this final report, we also demonstrate functional buried-heterostructure QCL devices in the MWIR, emitting near 4.5 μm. In parallel, we have also performed a field test of an eye-safe, amplitude-modulated, commercial QCL device at 4.0 μm, demonstrating up to 125 Mbps FSOC over a 1.6 km (1.0 mile) outdoor link.

Section 2 of this report gives an overview of a FSOC system, and describes experimental data collected to compare atmospheric conditions at 1.55 vs. 4.0 μm over a 1.6 km outdoor path during varied New England weather conditions. These parameters are summarized in terms of their impact on a full system link budget for a tactical-scale communication system, with ranges of up to tens of km.

Section 3 describes the selected laser architecture as it relates to high-speed modulation and amplification of QCL devices and how it can fit together in a future photonic integrated circuit platform, also under development at MIT LL. These future capabilities can address many of the current shortfalls of commercial mid-IR FSOC components, including narrowband, high-speed transmitters, filtering, and alternative detection schemes.

Section 4 reports on the current progress in developing MWIR QCL lasers and amplifiers at MIT LL for implementation with the architecture described in Section 3, summarizing epitaxial growth, buried-heterostructure regrowth, and facet coating recipes.

Section 5 describes an outdoor FSOC demonstration over a 1.6 km range, at rates of up to 125 Mbps.

2. MWIR FSOC SYSTEM STUDY

2.1 GENERAL SYSTEM OVERVIEW

To establish a high-bandwidth communications link, FSOC systems must solve several complicated problems simultaneously. Unlike most RF-based systems, they are highly directional and only operate within a clear line-of-sight path. Even without any atmospheric effects, this requires a pointing, acquisition, and tracking (PAT) sub-system to align the laser beams between transmitter and receiver. The data must be converted to and from the optical domain using transceivers (modulators and photo-detectors, respectively) using an appropriate modulation format. Frequently, additional optical amplification and signal conditioning must be included to improve the signal to noise ratio. A conceptual schematic of a general FSOC system is shown in Figure 1, below.

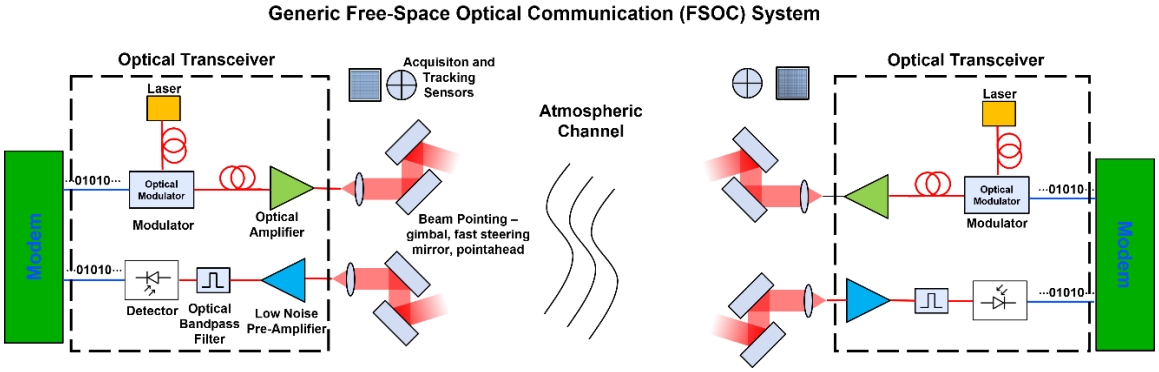

Figure 1. Layout of a generic FSOC system. Digital data in the electrical domain are converted by a modem to and from signals in the optical domain by transceivers (modulators and photodetectors), frequently with additional amplification and filtering. The optical channel is established and maintained via a pointing, acquisition, and tracking system.

Depending on the desired data rates and the constraints imposed by the desired platform, etc., the job of designing and implementing an FSOC system is thus particularly complicated. Many of the underlying technologies can vary significantly in performance from one wavelength to another. Fiber amplifier systems at 1.06 µm, for example, are now commercially available with several kW of output power, whereas similar systems at 1.55 µm are typically limited to 10 W. Both can be implemented with amplitude, phase, or frequency modulation, using electro-optic modulators with different formats that can be optimized for particular use conditions. Low-power systems in the 1 to 100 mW regime can typically use inexpensive laser diodes as transmitters, even without using additional modulator components, though frequently with a different set of constraints on modulation format. An MWIR implementation based on QCL technology will have its own unique set of trades, many of which have not yet been explored in the literature.

2.2 DUAL-WAVELENGTH ATMOSPHERIC MEASUREMENTS

To establish the more fundamental design trades between conventional NIR/SWIR and the MWIR wavelengths under consideration in this work—particularly as it relates to link budgets and PAT design—we built an atmospheric channel monitoring apparatus and operated it for several months under varying weather conditions in Lexington, MA. This setup consisted of a dual-band transmitter at 1.55 and 4.0 μm, collimated to ensure overlap over the 1.6 km optical path, and co-aligned using a dichroic. The receiver for the 1.55 μm beam consisted of a fast steering mirror and tracking camera, with a 12 mm diameter focusing lens to a detector. To aid in correlation to true atmospheric conditions, a commercial scintillometer was also aligned next to the 1.55 μm receive aperture. At 4.0 μm, the light was collected by a cored 3" diameter off-axis parabola to a Vigo PVI-4TE-5 MCT detector. The transmit and receive setups are shown in Figure 2.

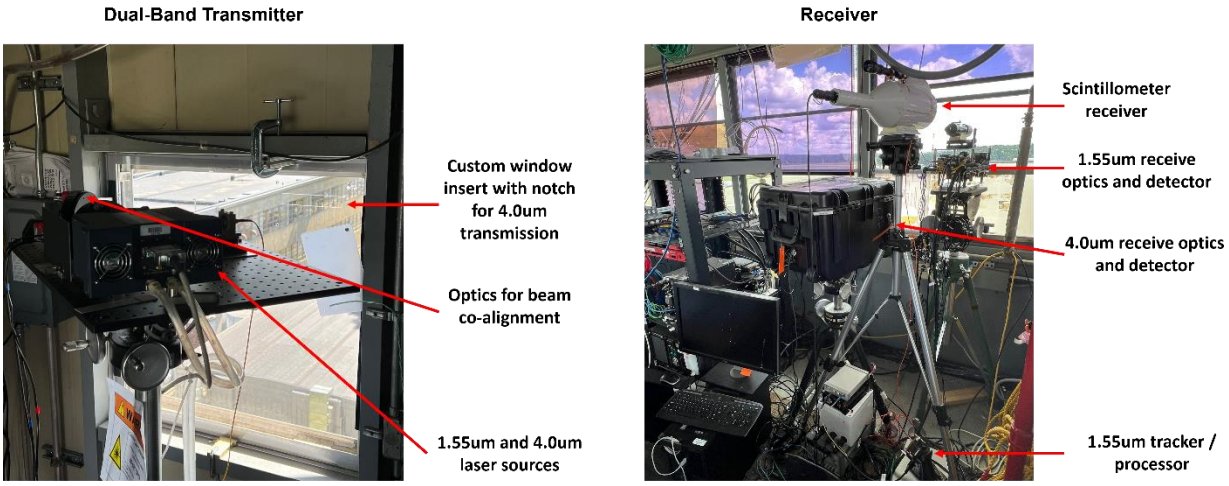

Figure 2. Dual-band atmospheric channel characterization setup at 1.55 and 4.0 μm.

The results of a typical data collection for a clear day in August are shown in Figure 3. For a given wavelength, turbulence typically reaches a maximum near solar noon and is minimized near sunrise and sunset. For the 4.0 μm channel, the scintillation index remains well below unity, within the Rytov limit, whereas the 1.55 μm channel shows large spikes into the strong turbulence regime during the middle of the day. The data shown are not corrected for aperture averaging, which creates a small additional advantage to the MWIR beam due to its larger (~1.9x) ratio of aperture diameter to turbulence-mediated spatial coherence length.

To qualitatively compare data collected during rainfall, we have generated histograms of the received signal power, with a typical example shown in Figure 4. The histograms had to be captured over a sufficiently short time that the average link extinction remained constant (e.g., rainfall rate and raindrop

size remained nearly constant) so as not to artificially broaden the histograms. It is well known that average extinction in light rain is less for MWIR than for NIR or SWIR. However, the stochastic nature of scattering due to rain droplets could potentially lead to enhanced irradiance fluctuations at the receiver, in addition to fluctuations due to the background turbulence effects. In all cases, the MWIR data show significantly less variation than SWIR and the measured log irradiance fluctuations are in line with those predicted from turbulence alone. In the weak turbulence regime (Rytov approximation), scintillation index (normalized variance of the received irradiance fluctuations) scales with wavelength$^{(-7/6)}$. This expression predicts the log variance at 4 μm would be 3.14 times less than at 1.55 μm, but there is an additional factor of ~2.5x for the aperture averaging in MWIR (the 2.5x factor would become unity if the MWIR Rx aperture were the same size as the SWIR Rx aperture or only slightly larger). The shapes of the histograms are also consistent with gamma–gamma distributions, which are known to be applicable for fitting turbulence-induced fluctuation histograms over a wide range of turbulence conditions. We believe the dominant effect in all of these data samples is turbulence, rather than rain. It would be challenging to design an experiment that could accurately quantify the rain-induced portion of the fluctuations due to the uncontrolled nature of the turbulence and rainfall on an outdoor link. Future measurements could be improved by using a modulated waveform with <100 nsec pulses to probe multiple scattering in the time domain, more similar to those used in the PRBS demonstration in Section 5 of this report.

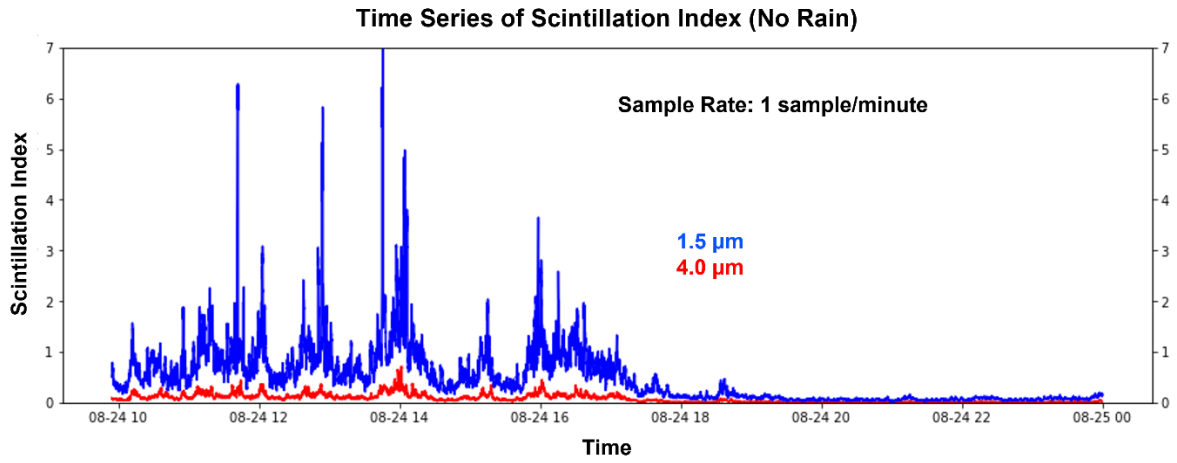

Figure 3. Time series data for a typical SWIR and MWIR data collect over the course of a clear day in August, showing a benefit to the longer wavelength.

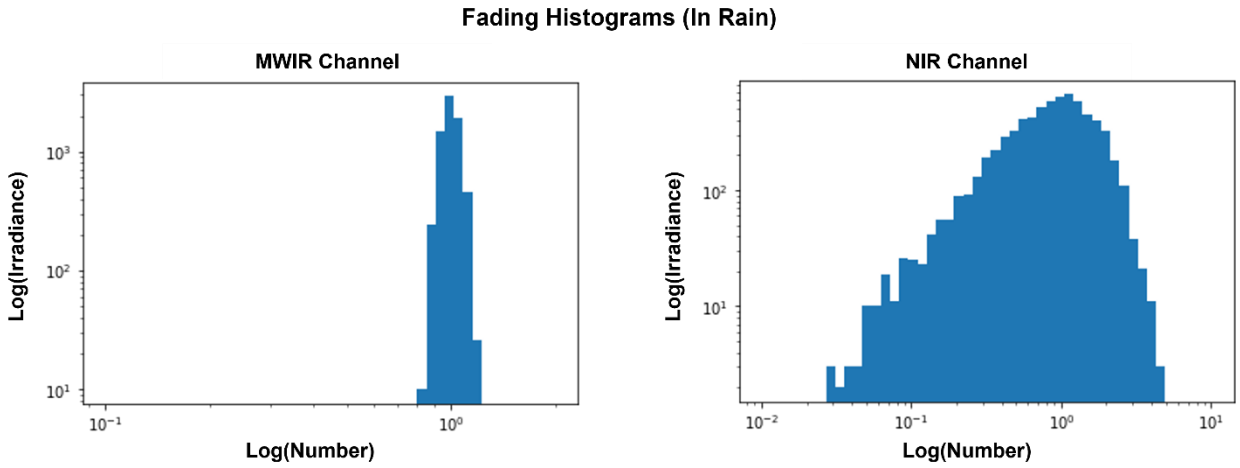

Figure 4. Fading histogram of MWIR and SWIR channels during rainfall, showing increased robustness to weather conditions at the longer wavelength.

2.3 FSOC LINK BUDGET ANALYSIS

It is useful to compare link budgets for SWIR and MWIR FSOC systems. As mentioned above, MWIR is well-suited to tactical environments due to better weather tolerance and relative immunity to fading/scintillation. The larger diffraction angle of MWIR is not a disadvantage for tactical links where link ranges are only tens of km and where platforms are maneuvering. Although a 1.55 μm long-range link might use beamwidths in the few tens of microradian range, a tactical system can benefit from beams of hundreds of microradian width, if the link budget permits. Another advantage is that QCL MOPA devices are able to output considerably more power (Watt class) than 1.55 μm DFB lasers (~10 mW), and therefore 1.55 μm systems need the additional SWaPC and thermal management of a Tx high-power optical amplifier (HPOA). Erbium-doped HPOAs are inefficient at 10–20% wall plug efficiency. The much weaker turbulence has the potential to be a huge advantage, not only because 1.55 μm turbulence mitigation techniques (which degrade SWaPC and add complexity) may not be necessary, but also because MWIR systems may be able to operate over longer distances.

Of course, SWIR systems benefit from the availability of a wide variety of COTS components developed for the fiber telecom industry, with the exception of some turbulence mitigation components and methods. Receiver performance is a major advantage in the SWIR for multiple reasons: (1) low-loss optical fibers enable narrow spatial filtering that rejects background, (2) narrowband optical filters (GHz-class) are readily available for spectrally filtering out noise and other wavelength multiplexed data streams (vs. 100 nm-class COTS filters in the MWIR; although solar background is less in MWIR), (3) very low noise-equivalent power (NEP) photodetectors with high bandwidth are available, (4) very low-noise (noise figure, NF ~3dB) optical fiber-based preamplifiers are commercially available and these, in conjunction with photodiodes, can provide nearly optical shot-noise-limited receiver performance. MWIR receivers, on the

other hand, cannot as effectively (spatially or spectrally) reject background light, and in MWIR, the receiver optical chain (unless cooled substantially) and channel generate MWIR blackbody radiation, a source of optical noise that is typically irrelevant in the SWIR. In addition to the added optical noise in MWIR, there is substantial electrical noise. An MWIR detector might have a NEP of ~200 pW/$\sqrt{Hz}$, whereas a 1.55 μm photodiode might have an NEP of 2 fW/$\sqrt{Hz}$, 5 orders of magnitude lower. This does have an impact on MWIR lasercom links by constraining the achievable (data rate)*(range^2) product, and nearly ensuring that non-preamplified direct detection will be far above the quantum limit. An exemplary MWIR detector, the Vigo InAsSb photovoltaic detector, PVIA-2TE-5-1x1-T08-wAl2O3-36, has a specific detectivity D* of ~4E10 cm-$\sqrt{Hz}$/W at its peak wavelength of 4.5 μm, 1mm × 1mm active area, and a time constant of <5 ns, making it suitable for up to nearly 100 Mbaud signaling. Detectivity D = D*/$\sqrt{area}$ = 4E11 $\sqrt{Hz}$/W. Inverting, we obtain the NEP = 2.5 pW/$\sqrt{Hz}$. For 100 MHz signaling bandwidth, this gives an NEP of 25 nW. NEP is defined for optical signal-to-noise ratio (OSNR) = 1. For an 18 dB OSNR, typical but conservative for a lasercom link (corresponds to an uncoded, OOK, detector-limited error rate of ~1E-13.7; but if we assume the modems run forward error correction (FEC) that can operate error-free at 1E-3 uncoded bit error rate, then we could relax the OSNR to 11.4 dB), the required signal level is 1.6 μW, which, though much higher than the minimum optical power required at 1.55 μm for the same data rate, is sufficient for many tactical links.

Next we summarize elements of a sample MWIR link budget. Scattering off the surfaces of the optical components in the Tx might account for 2 dB loss (between the output of the laser/amplifier/MOPA and free space). Physical losses in the Rx might be 5 dB, depending on the quality of the AR coatings, type of receiver, and coupling efficiencies. Rx tracking loss could be another dB. Beam-pointing bias is expected to be <1 dB and smaller than at 1.55 μm because of the wider beams used in MWIR, at least for CONOPS, that limit maneuver, but could be larger and time-varying with unpredictable maneuvers. Tx implementation loss accounts for imperfections in the transmitted waveforms, and this could lead to another 2 dB of net loss. Rx implementation loss likewise might add net 2 dB. Blackbody radiation from the Rx optics and channel (irrelevant at 1.55 μm) could in principle degrade the OSNR more than the detector, in which case cooling the Rx would be warranted. FEC postprocessing gain might be 1–9 dB. Of course the primary loss of signal power is diffraction—a 1 mrad beam at 10 km will be expanded to 10 meters wide, and for a 0.1m Rx aperture, this accounts for 37 dB of diffraction loss (3dB is retained because the receive aperture is capturing power at the peak of the Gaussian beam; there may be minor additional losses due to truncation of the beam in the Tx aperture). Let us suppose that the Tx optical power amplifier (or laser directly, if no amplifier) output is 1 W. Let us further suppose that the power is reduced by an aggregate 15 dB due to scattering, pointing, and other optical losses, and by another 37 dB diffraction loss at 10 km for a net 52 dB loss, and we are left with 6.4 nW of received power, which provides 6 dB margin above the OSNR target.

To extend to 100 km, another 20 dB is needed to make up for the additional diffraction loss. The most straightforward way to achieve this is to narrow the comm beam by a factor of 10 in linear angle. We assumed a 1 mrad beam for the 10 km example above. If we narrow the beam to 100 μrad, we arrive at the same net result, but over 100 km: 6.4 nW of received power, which provides 6 dB margin above the OSNR

target. The narrower beam makes pointing and tracking more challenging. For comparison, NASA's LCRD is able to send Gbps data over 37 Mm using beams roughly 5 times narrower than 100 microradians, but of course, as a geostationary satellite communicating with stationary ground terminals, maneuvering (other than predictable station keeping) is not an issue. There are other options for recapturing diffraction loss; increasing the Rx aperture diameter also provides a square-law improvement, but increases SWaPC. Strong FEC reduces the required OSNR.

We can identify technology investments that could further improve MWIR comm and PAT link budgets. If a QCL amplifier with >1W output power could be fabricated, then that additional power would directly provide a linear improvement in the link budget. A low-noise optical preamplifier, possibly also a QCA, could dramatically improve the link budget because the dominant noise in these links is the electronic detector noise. Just ~20–25 dB of net amplifier gain could extend the link from 10 km to 100 km while also maintaining a 1 mrad beam width.

We close this section by noting for context that it would be challenging to close a horizontal FSOC link at 100 km at 1.55 μm with modest-sized apertures in the lower atmosphere because the SWIR turbulence is so strong under those conditions. MWIR not only greatly reduces the communications penalty (or cost and complexity of mitigation schemes) associated with turbulence, it may extend the achievable range.

3. QCL MOPA DEVICES FOR HIGH-SPEED MODULATION

3.1 CONCEPT OVERVIEW

Interest in free-space communications in the mid-IR using direct semiconductor sources dates back to at least 2001–2002, with some of the first demonstrations of fieldable QCL laser sources [1], as a potential solution to the "last mile" problem of residential high-speed internet distribution [3]. The approach ultimately lost out to RF cell phone and 1.55 μm fiber optic networks, but has received more attention recently [4]–[8], as QCL technology has matured. Recent designs, however, have been limited in optical transmit power, with typical output in the range of 1–10 mW. To facilitate high-speed modulation while still maintaining narrow optical bandwidth, these implementations use a short-cavity distributed feedback (DFB) QCL, with direct electrical injection. As a result, scaling to higher power—and therefore to longer ranges—is limited. One of the core motivations of this project is to explore the concept of using a QCL in a MOPA configuration to boost the power. This could be done in a similar way to conventional SWIR systems, where a fiber amplifier might boost the power after a signal passes through a dedicated electro-optic modulator, but the high inherent speed of QC devices also offers the possibility of using the amplifier itself as an amplitude modulator. In this case, a very narrow (kHz linewidth) seed could be maintained separate from the modulated signal, opening a path to coherent detection and other more interesting architectures.

This flexibility of implementation is also well suited to pairing with a photonic integrated circuit (PIC) platform, where optical signals are routed around via passive waveguides with other optical components, such as filters, splitters, and modulators on the same chip. Such systems have been developed in the visible through SWIR wavelength bands using various material systems, including Si, SiN, or direct III–V semiconductors. So far, however, demonstrations in the MWIR have been limited due to challenges with materials that are transparent at appropriate wavelengths. With a partner, internally funded effort ("Midwave Infrared Integrated Photonics Platform"), MIT LL is leveraging extensive experience in this area to push into the 4–5 μm band using SiGe waveguides on a Si substrate. A notional description of this approach is shown in Figure 5, below.

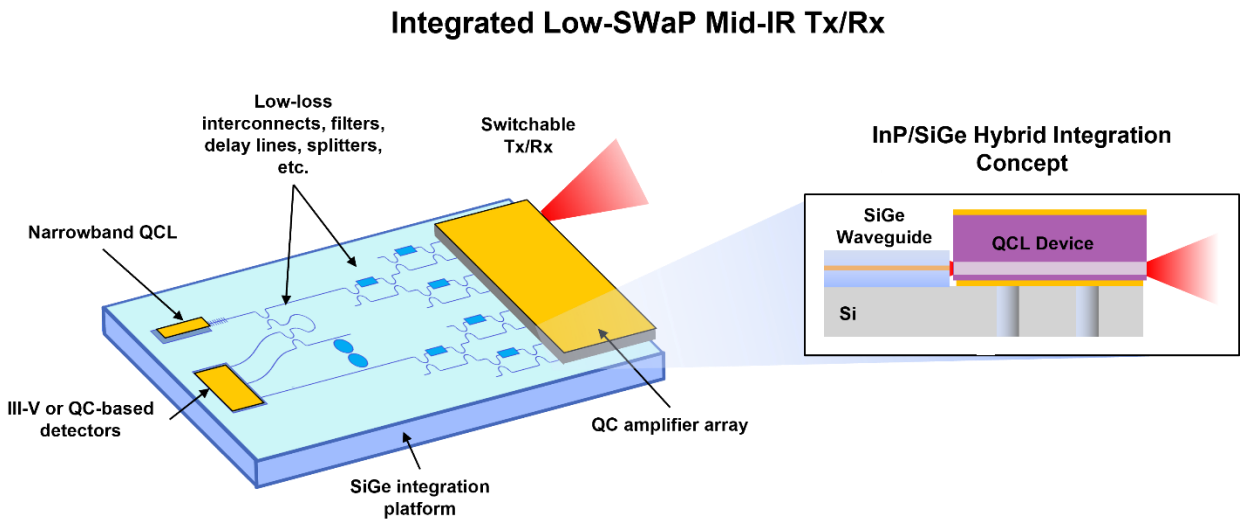

Figure 5. MWIR hybrid photonic integration concept, using QCL laser and amplifier insertion into a SiGe passive waveguide platform.

3.2 MOPA QCL PROOF-OF-PRINCIPLE TESTING

Our first demonstration of high-speed modulation using an amplifier is described in Figure 6. A low-power (~1 mW) continuous wave (CW) seed laser at a wavelength of around 9 μm is injected into an MIT LL-fabricated QCL device with anti-reflective (AR) coatings on both the front and back facets. The amplified beam is then mixed with a sample of the seed to allow for independent measurements of the imparted phase and amplitude modulation. The QC amplifier device is driven electrically with a combination of a DC current and a high-speed RF source, through a bias tee. At rates above ~1 MHz, the electrical current imparts a pure amplitude modulation on the device, with a measurable response up to 250 MHz, limited primarily by the metal contacts of the QC device. Significantly, the amplified output retains the spectral characteristics of the seed, up to at least tens of mW of output power. Further testing is required to ascertain if modulation at higher optical intensity could impart additional nonlinear effects (which may be either useful or deleterious).

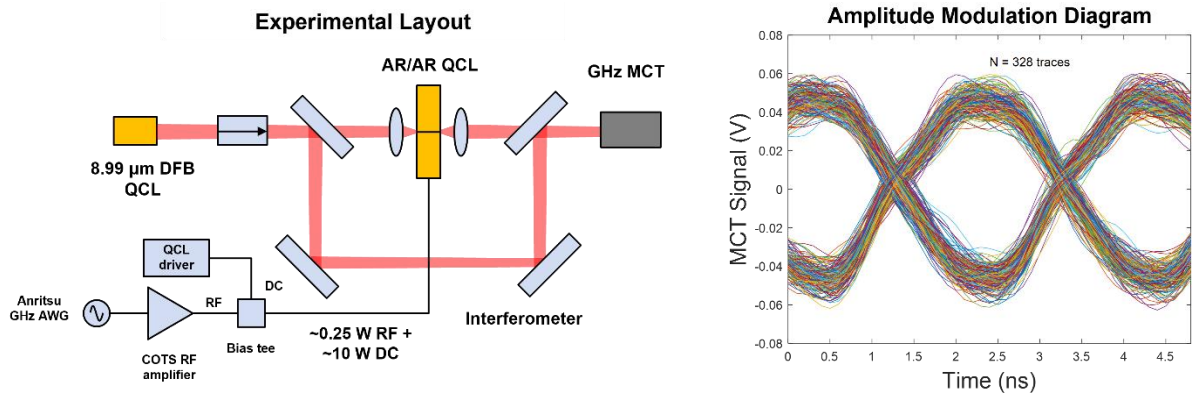

Figure 6. Experimental MOPA device testbed layout. Light from a DFB master oscillator is coupled into the device under test. The amplified output is combined with a sample of the input light to form an interferometer. The optical (phase and amplitude) response is then measured using MCT detectors while an electrical waveform is applied to the amplifier device.

This proof-of-principle test shows the promise of a MOPA approach for both modulation and signal amplification. In principle, FSOC systems in this LWIR wavelength band could be advantageous, for example, for short-range applications in deep turbulence or very dusty conditions, where improved atmospheric robustness would win out over larger beam divergence and high thermal background. Further development of the laser transmitter, however, faces several challenges. LWIR QCLs are inherently less efficient than optimized designs in the MWIR, and have a more limited set of appropriate optical coating materials, particularly those for facet anti-reflective coatings. As a result, the current devices oscillate on on-chip longitudinal modes before reaching their full output power and suffer from reduced lifetimes. The focus of our continued work, therefore, has been to develop similar devices operating between 4.0 and 5.0 µm.

This page intentionally left blank.

4. GROWTH AND FABRICATION OF MWIR QCL DEVICES

4.1 OVERVIEW

Prior to this work, growth and fabrication of QCLs at MIT LL had been primarily focused on LWIR devices, emitting between 8 and 9.5 μm. State-of-the-art active region designs in the MWIR have been shown in the literature to have significantly higher efficiencies than their long-wave derivatives [11], but are more difficult to grow, fabricate, and regrow for high-power continuous-wave operation, requiring careful calibration of alloy compositions for strain compensation and smaller feature sizes for supporting single-spatial-mode operation. Over the course of this project, we have demonstrated QCL epitaxial material covering the wavelength range from 4.0 to 5.0 μm, several with pulsed efficiencies on par with the best commercially available devices when fabricated as ridge waveguide lasers. We have developed procedures for buried heterostructure regrowth and demonstrated pulsed operation of sub-wavelength-scale waveguide lasers. In parallel, we have also developed an AR coating process to suppress on-chip lasing for application to a MOPA architecture and for insertion into MWIR PIC platforms.

4.2 MWIR QCL GROWTH AND REGROWTH

To cover the entire MWIR band, we chose to grow three active region designs. The shortest-wavelength version, for emission at 4.0 μm, was developed under a previous Line-funded effort led by Dominic Siriani in 2016 (“Novel High-Efficiency LWIR QCLs”). The other two, nominally centered at 4.3 and 4.6 μm, were taken from the open literature. Several variations on each design were grown by metal-organic vapor phase epitaxy (MOVPE), and then processed into simple wet-etched laser devices for pulsed light, current, and voltage (LIV) performance measurement. Simultaneous wavelength measurements were also taken using a Fourier-transform infrared (FTIR) spectrometer. The high-level results are shown below in Figure 7.

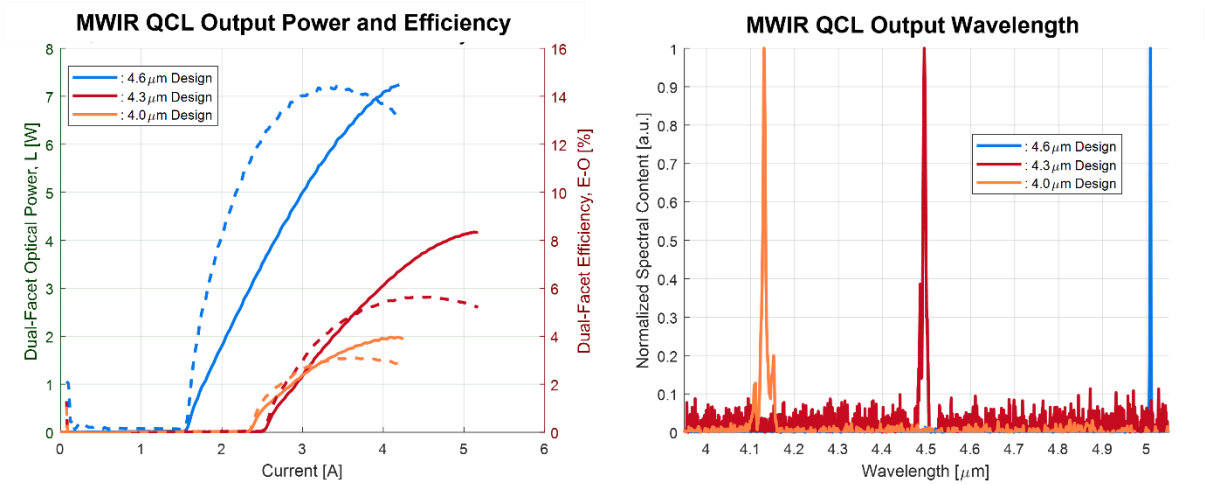

Figure 7. MIT LL MWIR QCL performance data for three different designs emitting at 4.1, 4.5, and 5.0 µm.

The next important challenge for high-power MWIR QCLs is fabricating a buried-heterostructure device. In order to maintain high efficiency and good beam quality in CW operation, the QCL waveguide must be etched to a narrow (wavelength-scale) width, and surrounded by thermally conductive, but electrically resistive and low-loss material. This is accomplished through Fe-doped InP regrowth. To accommodate the short wavelength, and therefore small feature sizes, of these devices compared to LWIR QCLs, we use a two-step regrowth approach. In this process, the initial epitaxial growth stops at the top of the active region. A 3–4 µm wide and deep etch can then be used to define the waveguide, and the sidewall covered in a layer of Fe:InP. The top cladding of conducting Si:InP is then grown as a second step. An example SEM image of a MWIR QCL is shown in Figure 8 with a corresponding pulsed LIV characterization.

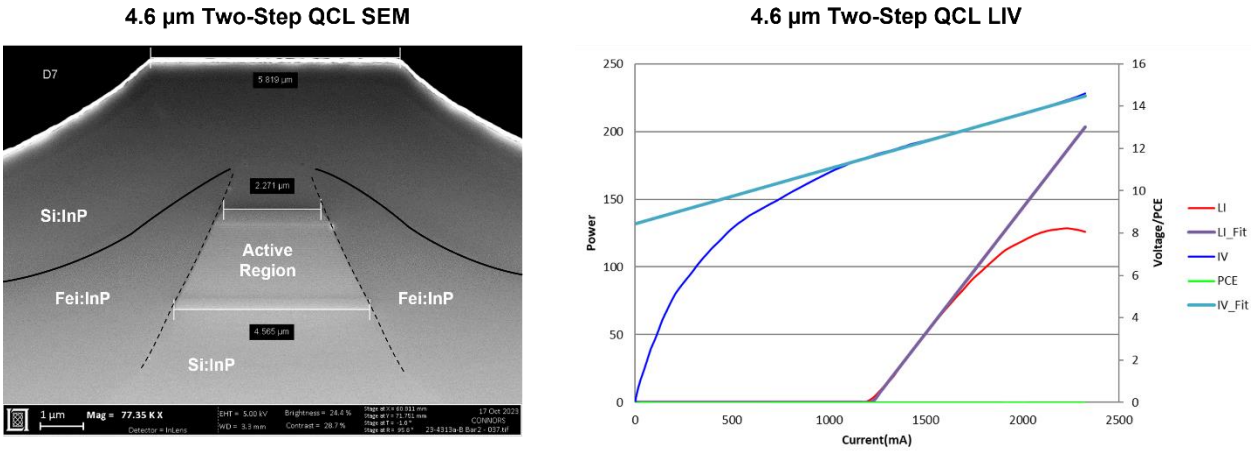

Figure 8. Buried heterostructure QCL fabricated with a two-step regrowth. The etch and regrowth boundaries are highlighted with dashed and solid lines, respectively. The waveguide width and Fe:InP regrowth depth are both ~4 µm. The pulsed-mode LIV curve for a selected 8 mm long device is shown to the right.

This device operates in a short-pulse mode; however, the threshold current density is approximately two times higher than the equivalent ridge waveguide devices. We believe this is due to a parallel current path via space-charge-limited conduction through the semi-insulating Fe:InP layer in the field between devices, which in this case is only 4 µm thick, consistent with a simple Mott-Gurney model. In future work, this leakage path can be removed, for example by etching it away, or by limiting the contact area above the device active region.

4.3 MWIR FACET AR COATING DEVELOPMENT

A robust facet coating recipe is critical for the development of anything but the most simple of QCL-based devices. For our purposes, AR coatings are necessary for suppressing on-chip longitudinal modes that would otherwise oscillate between the cleaved facets, which have an inherent Fresnel reflection of ~25%. A good AR with reflectivity below 1% enables optimized DFB lasers, and is critical for both single-pass MOPA devices and external cavity devices like those pursued by the integrated photonics Line program.

For this work, we are pursuing a simple AR coating with a desired reflectivity in the range of 1%. Critically, we need the coating to withstand the temperature cycling and stress associated with soldering the laser chip to a submount. This has been a particular challenge with long-wave IR QLCs we have fabricated in the past, as there are known adhesion issues with the limited number of materials that are transparent above a wavelength of 8 µm. This resulted in a large number of facet failures during CW laser operation. In the MWIR band, there are significantly more material options; however, there are still a number of parameters that need to be optimized to achieve acceptable performance. To this end, we selected

a simple, single-layer design, based on HfO_2. As a robust material that is highly transparent out to 5 μm, we expect this to be a good baseline design that could be altered as needed in the future.

A quarter-wave film of HfO_2 was applied to a fabricated 4.1 μm buried-heterostructure laser bar on only a single facet. By comparing the power emitted from the coated vs. uncoated sides, we derived the resulting reflectivity at around 0.5%, as shown in Figure 9. Coated devices were run through a thermal cycle compatible with soldering to a heatsink and showed no measurable change in performance.

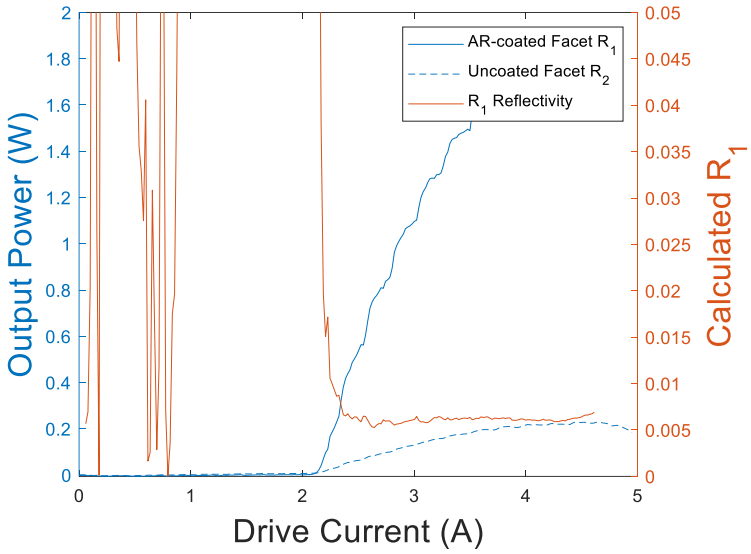

Figure 9. Calculated AR performance based on an internally developed method for extracting the facet reflectivity from measured front and back facet LIV data.

5. A 1.6-KM OUTDOOR MWIR FSOC DEMO

To date, most reported demonstrations of FSOC in the mid-IR bands have been performed in the laboratory, across link distances allowable by a single optical bench. Although some of these have reached >10 Gbps data rates, outdoor demonstrations and those longer than a few meters have been limited, with a severe penalty in bit rate. Figure 10 shows a summary of notable work, taken from references [6], [7], and [8]. There have also been some recent demonstrations using wavelength conversion from the SWIR band to the MWIR that have reached >100 Gbps, though still over meter-class distances [9], [10]. Wavelength conversion also adds significant complexity and SWaP to the Tx and Rx optics compared to the direct-semiconductor approach.

Wavelength (μm)	Data rate/bandwidth	Modulation Format	Channel (m)	Year	data rate*range^2 (Hz*m^2)
7.3	100 MHz	Analog	70	2001	49 x10^9
8.1	2.5 Gbps	NRZ-OOK	1	2001	2.5 x10^9
8.1	0.75 – 1.5 GHz	QPSK	100	2002	15 x10^{12}
9.3	350 MHz/115 kbps	Analog/NRZ-OOK	350	2001	43 x10^{12}
10.46	20 kHz	Pulse frequency	6000	2008	720 x10^9
4.7	40 MHz	Analog	2.5	2015	250 x10^6
4.65	3 Gbps	NRZ-OOK, PAM-4/8	.05	2017	7.5 x10^6
4.65	4 Gbps	PAM-4, DMT	.05	2017	10 x10^6
9	10 Gbps	OOK	0.7	2022	4.9 x10^9
9.6	11 Gbps	PAM-4	0.25	2022	690 x10^6
4.05	125 Mbps	OOK	1600	2023	320 x10^{12}

Figure 10. Recent summary of IR FSOC literature demonstrations. The first 8 rows adapted from reference [6]. Rows 9 and 10 are from references [7] and [8], respectively. The bottom row is this work.

To be of interest for tactical communications, an eventual FSOC system should be able to operate over distances of at least one to several tens of km. Here, we report an outdoor demonstration over a distance of 1.6 km (1.0 mile), using a PRBS7 test pattern at 50 to 125 Mbps at 4.05 μm. To our knowledge, this is the highest (data rate)*(range^2) product of any mid-IR FSOC performed to date.

For this demonstration, we worked to implement the MOPA-based concept described above, and we used a commercial Fabry-Perot QCL device from Thorlabs (part number QF4050C2) as the transmit laser. In the atmospheric band around 4 μm, narrow-line operation is not critical for high atmospheric transmission across long distances, so the frequency instability in a Fabry-Perot device can be largely neglected. For a 1" aperture, the eye-safe limit for operating near the ground is ~100 mW, which this device can readily achieve. For higher power per channel, data rate scaling via wavelength division multiplexing, or expanding into the more featured atmospheric transmission band from 4.5 to 5.0 μm, a MOPA transmitter with a well-controlled, nm-class linewidth would offer significant additional benefits.

The transmitter assembly is shown in Figure 11. The laser device is collimated with a custom-designed 1" diameter optical system, to produce a nearly-round 8 × 10 mm diameter beam with minimal astigmatism. The output is then folded onto a dichroic to allow co-boresighting with an MWIR camera. The entire assembly, with RF impedance matching, was then mounted on a tripod and pointed through a window to the receiver. The electrical drive setup is the same as that used in the MOPA testing, with a bias tee combining a DC current supply with an amplified RF signal.

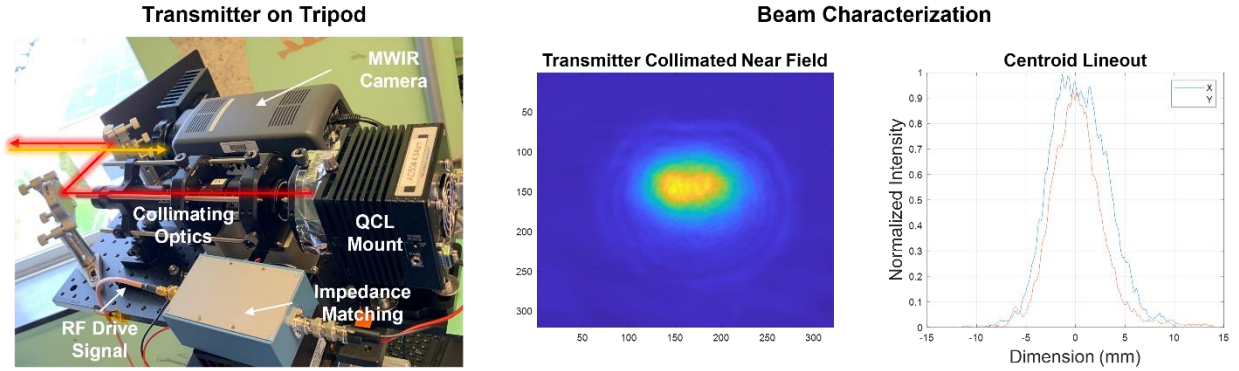

Figure 11. Transmitter assembly, composed of a QCL device, with collimating optics, overlapped with the field of view of an MWIR camera using a dichroic. The output beam was characterized on a pyroelectric beam profiler, with a beam major axes of 8 × 10 mm.

The link geometry is shown in Figure 12. The transmitter was pointed out of a window on the MIT LL campus in Lexington, MA, with the receiver placed on the roof of the Flight Test Facility building on Hanscom Air Force Base. The building housing the receiver optics is ~8 m wide.

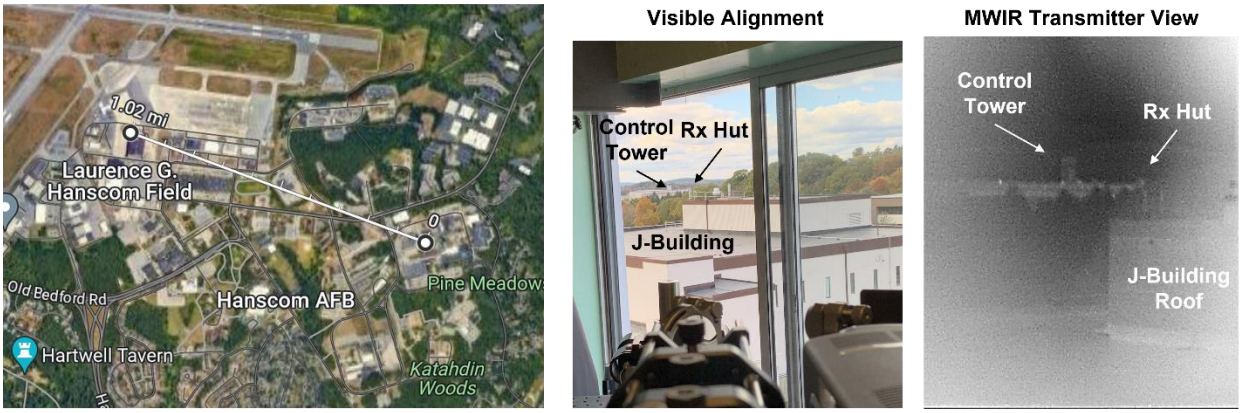

Figure 12. A 1.6 km (1.0 mile) link geometry with the visible and MWIR view from the transmitter location.

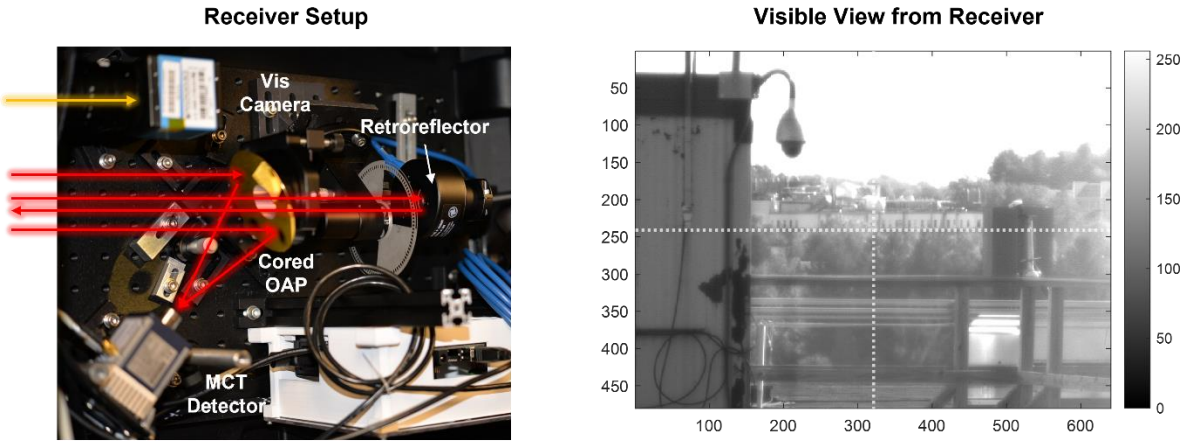

Figure 13. Layout of FSOC receiver. Light is collected by a cored off-axis parabola (OAP) and focused onto a high-speed detector. A co-aligned visible camera and a retro-reflector help with manual alignment.

The receiver optical setup is shown in Figure 13. The layout is the same as that used in the atmospheric monitoring setup described above, except that the detector is replaced with a higher-speed Vigo PVI-4TE with a 200 MHz programmable pre-amplifier. Consistent with previous scintillation data, no active control is required to maintain alignment, and the received signal level is stable over each 200 µs data collect. By sweeping the transmitter pointing back and forth across the building housing the receiver, we could confirm that the received and retro-reflected signal faded in and out, consistent with a 10 mm diameter Gaussian beam propagated to a distance of 1.6 km (~8 m diameter).

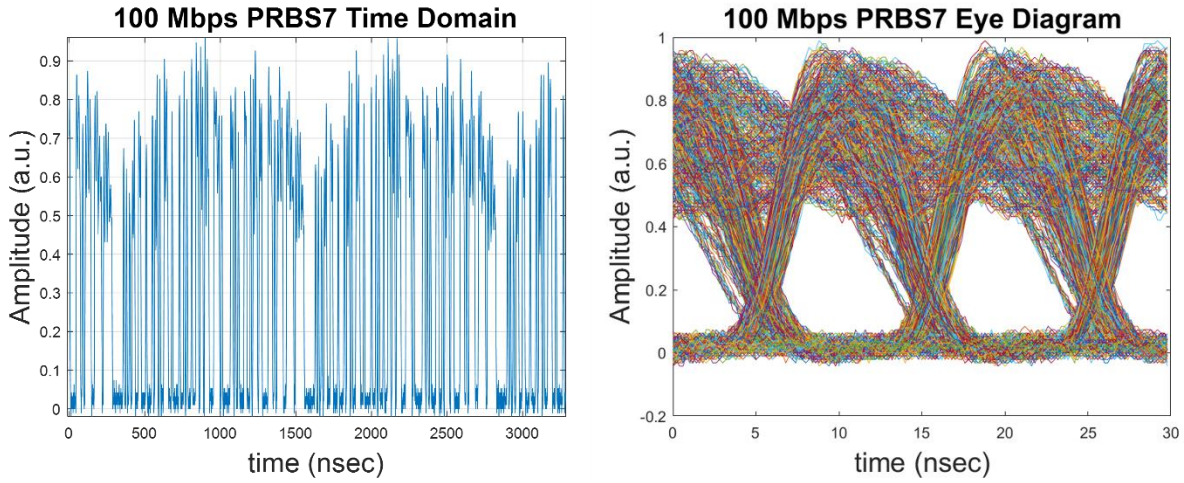

Figure 14. Time-domain trace and eye diagram for an OOK amplitude-modulated PRBS7 test pattern at 100 Mbps. The noise is highly repeatable and dominated by the RF drive circuitry and detector response.

An example 100 Mbps time-domain data trace with associated eye diagram is shown in Figure 14. Data were collected across two clear-weather days at ~20°C between the hours of 1000 and 1600 (maximum turbulence). A PRBS7 signal was used as a test pattern, generating a simple on–off keyed (OOK) amplitude modulation of the optical signal. There is significant noise on top of the received pulses, which partly closes the resulting eye. This noise is repeated across the entire 200 µs trace and is not associated with either atmospheric effects or receiver noise. It is likely a result of the specific frequency response of the RF amplifier. Channel equalization like that performed in reference [4] could reduce this noise significantly and enable multi-level pulse amplitude modulation (PAM) formatting, increasing the achievable data rate to Gbps. Improved device contacting could also increase the analog bandwidth of the laser itself, as it is not limited by the inherent electron lifetime within the QCL active region, which is typically in the 10 picosecond regime.

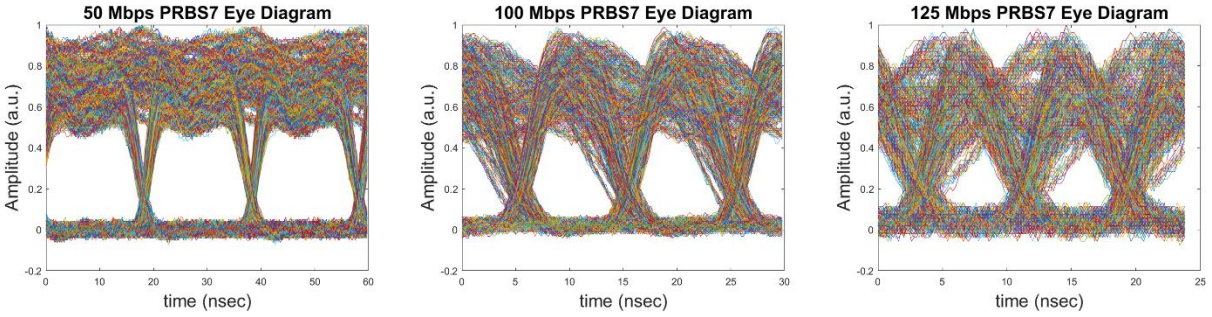

Figure 15. Eye diagrams for a range of bit rates, from 50 to 125 Mbps with a PRBS7 test pattern. Higher and lower rates are limited by the bandwidth of the implemented RF electronics. No channel equalization was performed.

Data were collected over a range of bitrates, with resulting eye diagrams shown in Figure 15. The lower bandwidth limit for the RF electronics is set by the RF amplifier and the capacitance of the bias tee, and was ~1 MHz in this work. At 50 Mbps, the lowest-frequency components begin to see significantly different gain than the high-frequency ones, resulting in an apparent closing of the eye. Similarly, the upper frequency bound is set by the RF amplifier, the electrical traces and wire bonds leading to the QCL, and the response of the MCT detector, all of which were ~200 MHz, limiting the PRBS rate to 125 Mbps.

This page intentionally left blank.

6. CONCLUSIONS AND NEXT STEPS

In this work, we have demonstrated the basic viability of tactical FSOC systems operating in the MWIR spectral region based on QCL lasers as high-speed, amplitude-modulated transmitters. Direct atmospheric measurements show a clear benefit in terms of scintillation and fading effects to operating at wavelengths longer than the typical 1.55 μm telecom band. As a proof of principle, we have demonstrated an example link at 125 Mbps over a distance of 1.6 km, using a transmitted power of 100 mW at 4.05 μm. To our knowledge, this is the highest (data rate)*(range^2) product demonstrated to date in the mid-IR. Link budget analyses show that although there are different relevant parameters compared to conventional wavelengths in terms of beam divergence and noise factors, Gbps data rates are possible up to tens of km ranges, relevant to many ground-to-ground, ground-to-air, and air-to-air scenarios.

Future work will focus on increasing the transmit power of QCL devices using a MOPA-based architecture. We have shown that a single-pass amplifier QC device can act as both a power amplifier and a high-speed modulator while maintaining narrow linewidth, and have developed the critical processes for implementing this architecture in the MWIR. Further measurements of QCL MOPA devices as high-gain, low-noise pre-amplifiers in the nW power regime could also enable new architectures with improved link budgets. Integration with a passive waveguide platform—also under development at MIT LL—can also offer a set of other features not available commercially in this wavelength band, including signal routing, splitting, and narrowband optical filtering.

This page intentionally left blank.

REFERENCES

[1] Corrigan, Paul, et al. "Quantum cascade lasers and the Kruse model in free space optical communication." *Optics Express* 17.6 (2009): 4355-4359.

[2] Martini, R., et al. "Free-space optical transmission of multimedia satellite data streams using mid-infrared quantum cascade lasers." Electronics Letters 38.4 (2002): 181-183.

[3] Acampora, Anthony. "Last mile by laser." Scientific American 287.1 (2002): 48-53.

[4] Pang, Xiaodan, et al. "Direct modulation and free-space transmissions of up to 6 Gbps multilevel signals with a 4.65-$\mu $ m quantum cascade laser at room temperature." Journal of Lightwave Technology 40.8 (2022): 2370-2377.

[5] Joharifar, Mahdieh, et al. "High-speed 9.6-μm long-wave infrared free-space transmission with a directly-modulated QCL and a fully-passive QCD." Journal of Lightwave Technology 41.4 (2023): 1087-1094.

[6] Pang, Xiaodan, et al. "Free-Space Communications Enabled by Quantum Cascade Lasers." *physica status solidi (a)* 218.3 (2021): 2000407.

[7] Dely, Hamza, et al. "10 Gbit s− 1 free space data transmission at 9 μm wavelength with unipolar quantum optoelectronics." *Laser & Photonics Reviews* 16.2 (2022): 2100414.

[8] Joharifar, Mahdieh, et al. "High-speed 9.6-μm long-wave infrared free-space transmission with a directly-modulated QCL and a fully-passive QCD." *Journal of Lightwave Technology* 41.4 (2023): 1087-1094.

[9] Zou, Kaiheng, et al. "High-capacity free-space optical communications using wavelength-and mode-division-multiplexing in the mid-infrared region." Nature Communications 13.1 (2022): 7662.

[10] Su, Yulong, et al. "150 Gbps multi-wavelength FSO transmission with 25-GHz ITU-T grid in the mid-infrared region." Optics Express 31.9 (2023): 15156-15169.

[11] Razeghi, Manijeh, et al. "Recent advances in mid infrared (3-5μm) Quantum Cascade Lasers." Optical Materials Express 3.11 (2013): 1872-1884.

This page intentionally left blank.

ACKNOWLEDGMENTS

The authors are grateful for the contributions of John Taylor, Rdan Golden-Castano, Richard Garner, Keith Berkins, Alicia Volpicelli, Raksa Tan, William Spencer, Connor Brown, Jonathan Wilson, Anthony Esperti, Antonio Sanchez-Rubio, and Jason Stewart.

This page intentionally left blank.